We are IntechOpen, the world's leading publisher of Open Access books Built by scientists, for scientists

6,900
Open access books available

185,000
International authors and editors

200M
Downloads

Our authors are among the

154
Countries delivered to

TOP 1%
most cited scientists

12.2%
Contributors from top 500 universities



WEB OF SCIENCE™

Selection of our books indexed in the Book Citation Index in Web of Science™ Core Collection (BKCI)

Interested in publishing with us?
Contact book.department@intechopen.com

Numbers displayed above are based on latest data collected.
For more information visit www.intechopen.com



9

Joining of shape memory alloys

Odd M. Akselsen
SINTEF Materials and Chemistry
Norway

1. Introduction

Shape memory alloys (SMA) have received extensive attention in the last decades due to their unique shape memory effect (Miyazaki et al, 1981), pseudo-elasticity (Miyazaki et al, 1982; Miyazaki et al, 1986), excellent corrosion properties and very good biocompatibility (Sabur et al, 1984; Takei et al, 1983; Zhi et al, 2003). So far, they have been mainly used as functional materials, with medical/biomedical applications as prime example (Morgan, 2004). When adding their ability of "learning", as well as combining the function of a sensor, actuator or that of a construction (static) material, these alloys are placed in the next higher category, the "smart" materials. Since the shape memory effect in NiTi alloys, which covers 99.99% of the market today, was discovered as late as the 1960's (Buehler & Wiley, 1965), the potential of these alloys still has not been fully understood among designers and product developers in the materials industry. Now, their use have extended to new applications in the automotive industry (e.g. diesel fuel injector), MEMS (micro-electromechanical devices), aerospace and power plants (Wu & Schetky, 2000). Moreover, SMA has been gradually introduced to the civil engineering segment, where their ability as actuators, passive energy dissipaters dampers for civil structure control have been utilized (Song et al, 2006; Janke et al, 2005). Large structures as buildings and bridges can be exposed to severe vibration, which may introduce dangerous stresses. SMA tendons may be applied to modify structures to sustain high levels of seismic vibration. By strategic placement of such tendons, structural damage may be minimized during an earthquake. This principle has also been used to preserve architectural heritage in seismic areas.

In spite of recent landmarks in SMA applications, a limiting factor in further application is their poor machinability, which often sets limits to the freedom in design. Another factor is the lack of available joining techniques, particularly for joining of SMA to other materials. Although the subject has gained more focus lately, there are still quite few publications dealing with joining as regards systematic variations in joining parameters. Moreover, the requirements set to the alloy itself should also be approached, or even better, matched after joining. The accomplishment of sound joints is very challenging, since it is not limited to the joint strength, but also comprises the shape memory effect and pseudo-elasticity.

The present report is worked out to point some focus towards challenges and recent findings in the area of joining shape memory alloys, both to themselves and to other metals.

The joining processes evaluated are arc welding, beam welding and various solid state techniques. As will be shown, all joining techniques that involve heat to the base metals tend generally to cause reduction of their initial properties, but the most severe reduction in shape and superelasticity recovery is achieved in arc welding. In joining SMA to other metals, formation of brittle intermetallic compounds is difficult to avoid.

2. Types of alloys

There are mainly three groups of SMA represented in joining research and development work:

i. Ni-Ti alloys
ii. Cu-Al alloys and
iii. Fe-Mn alloys

The NiTi alloys dominate the commercial market, because of their larger shape memory effect and better pseudoelasticity. They have superior properties with respect to ductility, fatigue, corrosion resistance, biocompatibility and recoverable strain. The Fe-Mn alloys are by far the cheapest (Janke et al, 2005), which may cause an increased market interest in them. Other alloys may also be of future interest; especially alloys with higher phase transformation temperatures will represent a supplement to the existing ones, broadening the temperature range for application of SMA. Due to the greatest attention, the current report contains most information from joining of NiTi alloys.

3. Characteristic features of SMA

When e.g. Ni-Ti is subjected to high temperature, it consists of austenite with a body centred cubic lattice, while on cooling the austenite transforms to martensite with monoclinic lattice through a displacive shear transformation. Thus, independent of alloy system, the following temperatures can be defined:

M_s = start temperature for martensite transformation on cooling
M_f = finish of martensite transformation
A_s = start temperature for austenite transformation on heating
A_f = finish of austenite transformation

The driving force for this transformation is the difference in Gibbs energy between the two phases of martensite and austenite, and depends on both the temperature and the level of externally induced stresses. These two factors are also playing the main role in the transformation mechanisms and represent the origin of the shape memory effect (SME) and superelasticity[a] (SE). The first effect, SME, is defined as a phenomenon such that an apparent plastic strain given at a temperature below A_s recovers by heating to a temperature above A_f, by virtue of the (crystallographically) reversible reverse transformation. The typical stress-strain curve of a SMA is shown in Fig. 1 as the dashed line. At the end of a

[a] Superelasticity and pseudo-elasticity are equivalent terms; both are being used.

mechanical loading-unloading path (OBC) performed at constant temperature, the material presents residual deformation (OC). However, this deformation is not caused by dislocation movement, as it is in normal metal, but by detwinning of the martensite. Therefore, the residual strain may be recovered by heating of the material (CDO), as the material transforms from martensite to austenite. SE, which is a pseudoelasticity occurring at a temperature above A_f, is caused by stress induced martensite transformation upon loading and by subsequent reverse transformation upon unloading. This crystallographic reversibility, as shown in Fig. 1 by a dashed line, is characteristic of the thermoelastic martensite transformation, which is described by a small temperature hysteresis (i.e., $\Delta T = A_f - M_s$) and mobile austenite-martensite interfaces (Saadat et al, 2002).

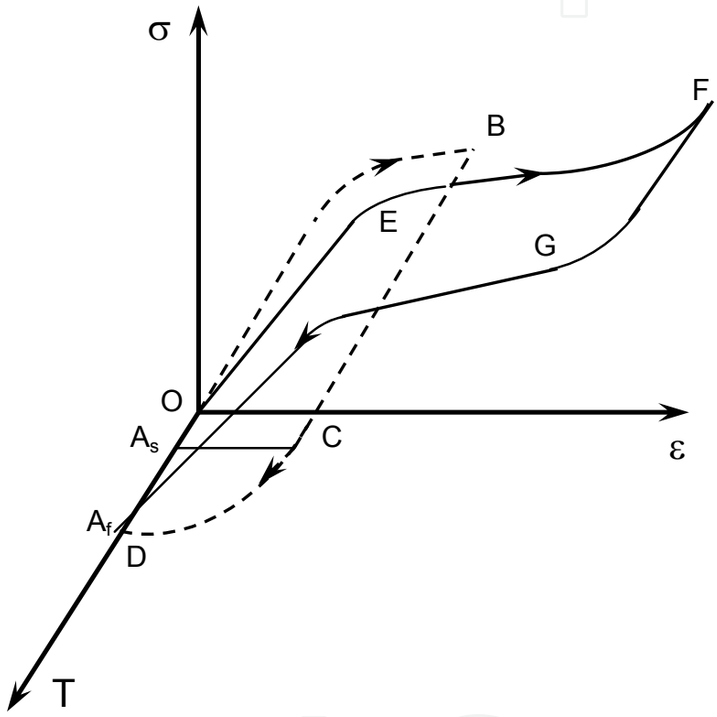


Fig. 1. Schematic stress-strain curve illustrating the shape memory effect (OBCDO) and superelasticity (DEFGD) (van der Eijk et al, 2004a).

In designing smart components in SMA, it is important to control the phase transformation temperatures in order to have the desired properties for a specific application. In Fig. 2, a schematic deformation map for a SMA showing stress-strain-phase transformation relationship. Here, M_d denotes the highest temperature below which martensite transformation can be induced by stress. Above M_d, SMA behaves like normal intermetallic compounds with CsCl-structure in which plastic deformation of the austenite occurs without inducing martensite deformation.

As indicated, the metallurgical and mechanical basics of SMA are well developed and understood. So far, however, their applicability has been limited due the lack of available fabrication techniques. Included are joining processes for assembling SMA to themselves,

and not at least, to other materials. The development of such cost efficient and quality processes will probably be the key to further increase in the engineering applications of SMA. In the present report, it will be demonstrated that such joining techniques are now extensively examined, primarily for NiTi alloys, but also for other alloys such as Cu-based and more recently, Fe-based SMA. It will be shown that some processes are very promising, but also that there is more work needed to be able to maintain the initial base material properties. In fact, it may be wise to include the joining in the design for certain applications, where shape memory effect or superelasticity is of primary concern. Such conceptual design will be much more cost effective since it may be possible to integrate alloy manufacture and joining operations.

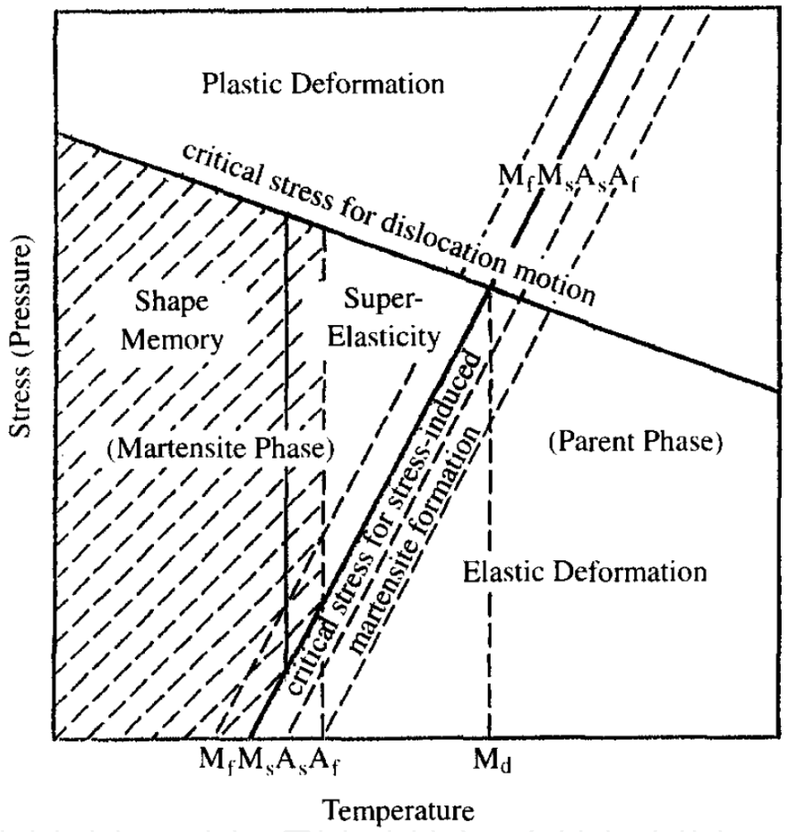


Fig. 2. Schematic deformation map illustrating phase stability, transformation temperatures and critical stress (Hosoda et al, 1998).

4. Arc welding

In the case of welding SMA, the properties to be matched between the base metal and the joint are the chemical composition and the microstructure, which dictates the shape memory response. This is where, fundamentally, the joining of SMA deviates from that of conventional metals such as steel, aluminium and titanium. In conventional alloys, successful joints are obtained in spite of differences in the chemical compositions and the microstructure of weld metal and heat affected zone (HAZ) on one hand, and the base metal

on the other. In welding SMA, this may not be the case, matching of chemical composition and microstructure, as well as transformation temperatures, is very important, since this controls the mechanical properties and the behaviour of the joint.

There are many arc welding processes available, but a very limited number of them have been tested for SMA. Due to the absence of adequate welding consumables, welding has been performed by gas tungsten (GTAW) or plasma arc welding (PAW), both being carried out without welding wire. Unlike gas metal arc welding (GMAW), these do not depend on the use of melting wire since the arc is established between a non-consumable tungsten electrode and the workpiece. During arc welding of SMA, embrittlement may occur due to the reactions with oxygen, nitrogen and hydrogen at high temperatures. Proper use of shielding and backing gas may thus be vital criterion to obtain sound welds. In addition, precipitation of brittle intermetallic compounds such as $NiTi_2$ and Ni_3Ti during solidification of NiTi SMA can have adverse effects on both strength and shape memory characteristics of the material (Shinoda et al, 1991). An example is contained in Fig. 3 for autogeneous plasma arc welding of NiTi, indicating a dramatic strength reduction after welding (van der Eijk et al, 2003). Similar results have been found in GTAW. Post weld heat treatment and training of the weld area is necessary to recover the shape memory effect after welding (Ikai et al, 1999). When welding NiTi to other metals, the formation of brittle intermetallic compounds may reduce the initial properties, Fig. 4. A number of different phases are distinguishable, as shown by the SEM backscattered image of the Hastelloy side. The composition of both sides of the weld was examined by electron dispersive spectroscopy (EDS) analyses. Here, six different phases were observed, having a wide range of chemical composition.

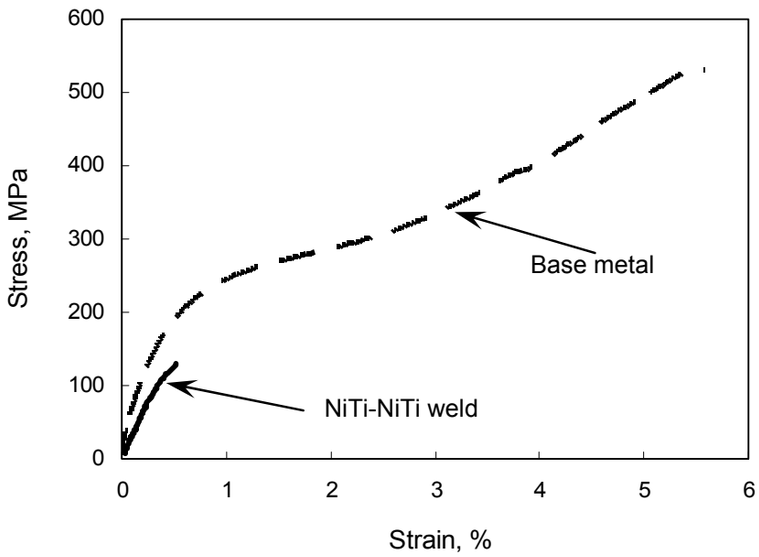
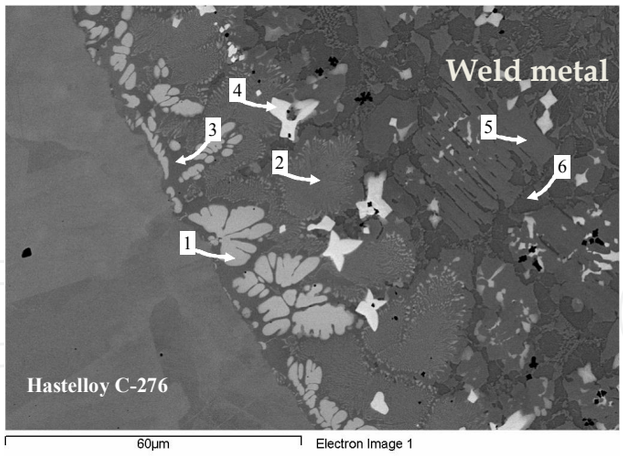


Fig. 3. Stress-strain curve of NiTi before (full line) and after GTA welding (dotted line) (van der Eijk, 2004b).



No.	Ni	Ti	Cr	Fe	Mo	W	Zr	Mn
1	30.3	4.4	20.7	4.2	30.7	9.6		
2	58.9	15.1	11.1	3.5	9.6	1.8		
3	68.4	16.3	7.3	3.1	3.8	1.6		
4	3.5	6.7	9.5		52.4	26.5	1.5	
5	75.5	21.8	1.4	1.3				
6	55.1	33.1	5.7	3.3	2.3			0.6

Fig. 4. SEM backscattered image of the fusion line of the NiTi/Hastelloy C-276 weld (van der Eijk, 2003) with corresponding EDS (wt%) analysis.

NiTi has a lower melting point (~ 1310°C) than Hastelloy C-276 (~ 1370°C) which can explain the absorption of elements from the superalloy into the NiTi. In addition, the different physical and mechanical properties may result in excessive thermal stresses and strains, and substantial cracking may occur, as shown for a plasma arc weld in Fig. 5.

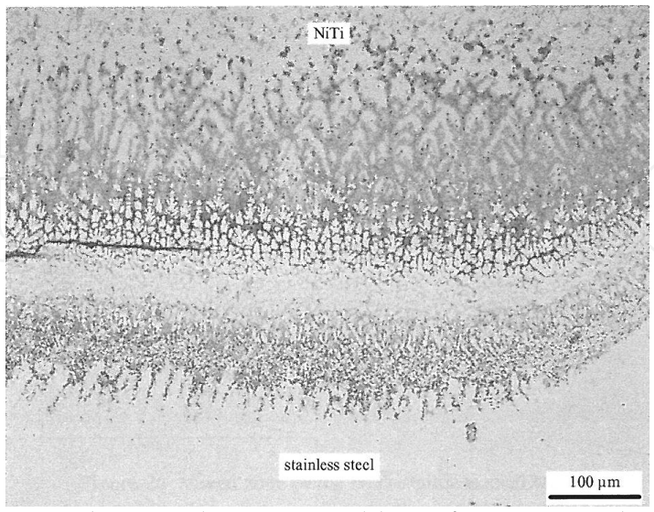


Fig. 5. Transition zone cracking in plasma arc welding of NiTi to stainless steel (van der Eijk, 2004b).

As discussed in the introduction part, the phase transformation temperatures may change in welding, which may restrict the application range of the alloy, or simply reduce its functionality. An example is contained in Table 1, showing values of M_s, M_f, A_s and A_f before and after welding. It is particularly the completion of transformation that changes due to welding, i.e., the M_f is lowered (30°C) and A_f is increased (16°C), resulting in a more sluggish phase transformation.

Welding method	Alloy	A_s (°C)	A_f (°C)	M_s (°C)	M_f (°C)
TIG (van der Eijk, 2004b)	Base metal	63	98	53	*35*
	Fused metal	59	114	65	*5*
Laser beam (Falvo et al, 2005)	Base metal	67	93	44	*10*
	Fused metal	*81*	*115*	*70*	*35*

Table 1. Results from DSC measurements of base metal and fused metal in NiTi/NiTi welds.

5. Beam welding

Laser beam welding results in narrower weld zones than arc welding (Pfeifer et al, 2008), as illustrated in Fig. 6. Both CO_2 gas laser (Tuissi et al, 2003; Hsu et al, 2001) and more extensively Nd:YAG solid state laser (Schlossmacher et al, 1994; Schlossmacher et al, 1997a; Schlossmacher et al, 1997b; Haas & Schüssler, 1999; Tuissi et al, 1999; Yan et al, 2006; Gugel et al, 2008; Khan er al, 2008; Song et al, 2008; Maletta et al, 2009) have been used. The Nd:YAG laser may give smaller welding spots and higher penetration depth than CO_2 laser since the plasma shielding effect is reduced due to the shorter wavelength (Haas et al, 1999).

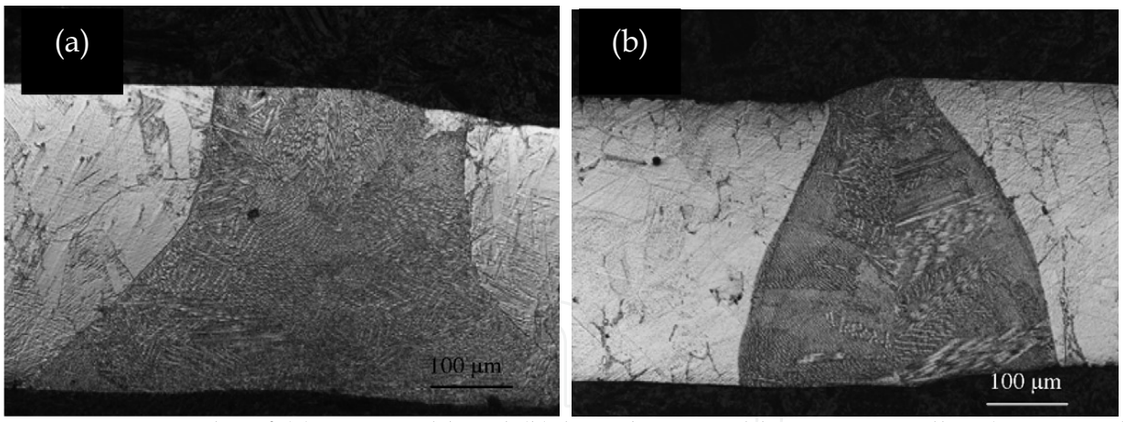


Fig. 6. Macrographs of (a) GTA weld and (b) laser beam weld; FeMnSiCr alloy (Dong et al, 2006).

As for arc welding, gas shielding is important to protect the fused metal against reaction with oxygen, nitrogen and hydrogen. Moreover, the weld quality will depend on the welding parameters (power, travel speed). The effect of laser power on minimum weld width is illustrated in Fig. 7, where the width is increased around 200 µm when the power is raised from 0.6 to 0.9 kW. The width of the fused zone, and the HAZ, is important for the thermal stresses and strains (usually called residual stresses and strains) which tend to increase with increasing width due to the larger volume to expand during heating and

contract during cooling. With lower heat input, an associated finer microstructure will be expected. This should help strength enhancement through the Hall-Petch relationship. However, as for arc welding, the strength reduction may be quite severe, as illustrated in Fig. 8. The fracture took place in the weld region.

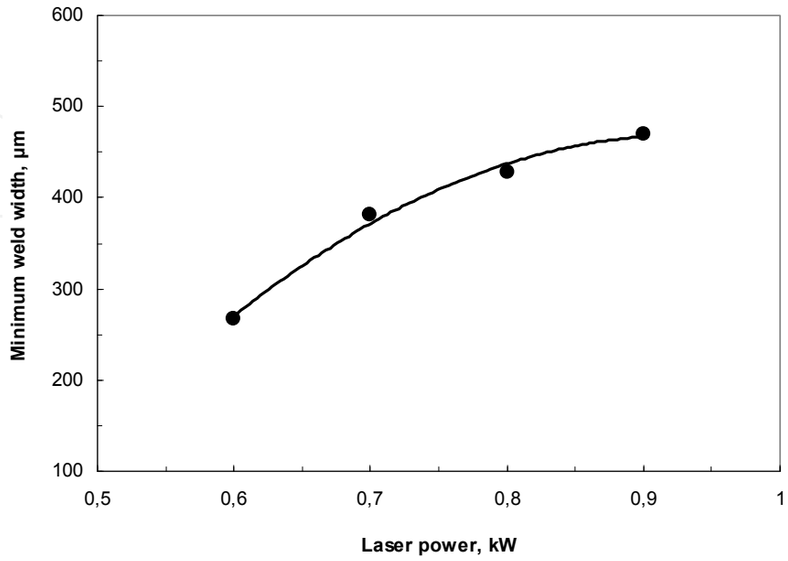


Fig. 7. Effect of laser power on minimum weld width (Khan et al, 2008).

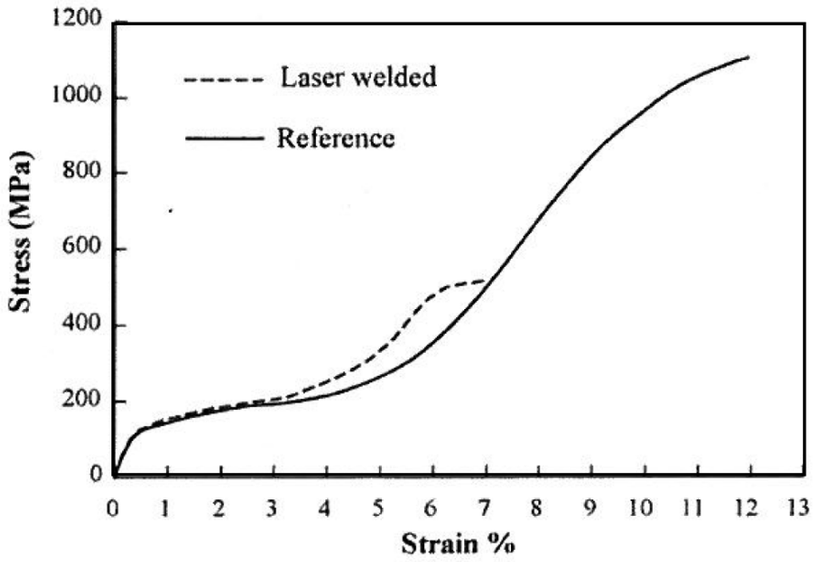


Fig. 8. Tensile stress-strain curve of NiTi before (full line) and after laser welding (dotted line). (Falvo et al, 2005).

The as welded properties can be improved by training. This point is outlined in Fig. 9, showing the measured two way shape memory strain ε_{tw}, recovery strain ε_{re} and plastic strain ε_p versus the number of training cycles before and after welding. It is seen for the base metal (filled symbols) that all strain types increase with increasing number of training cycles.

After welding, the behaviour is somewhat different. It appears that the two way shape memory strain ε_{tw}, and the recovery strain, $\varepsilon_{re,}$ pass through a maximum at 5 training cycles. Beyond 5 cycles, these strains are reduced, while the plastic strain, $\varepsilon_{re,}$ continuously increases.

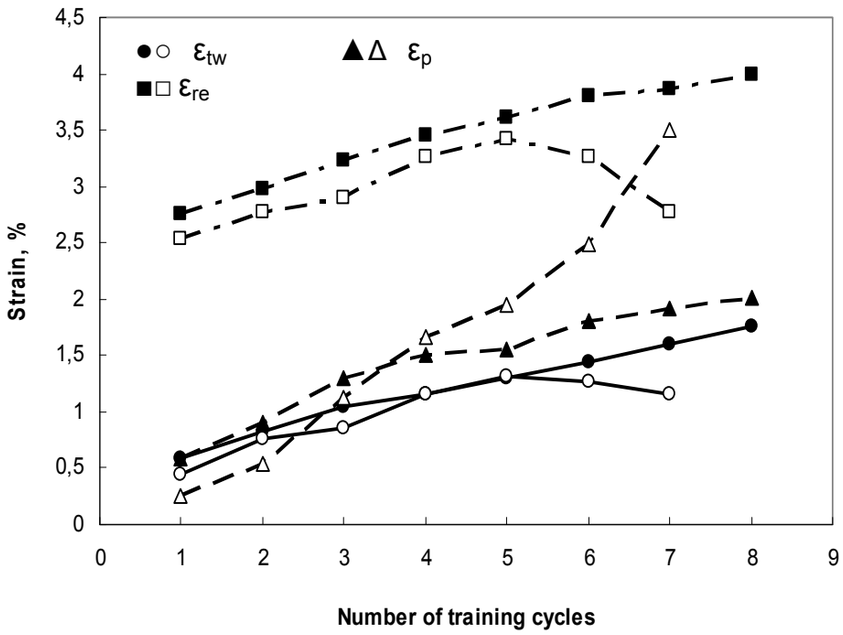


Fig. 9. Effect of training cycles on shape memory behaviour and plastic strain of NiTi alloy. Filled symbols: Base metal; Open symbols: After laser welding. (Falvo et al, 2008).

Beside the changes in mechanical properties following welding, a shift in the phase transformation temperatures (martensite to austenite and austenite to martensite) may take place. This may reduce the service temperature window for the SMA components. Phase transformation data for laser welding are listed in Table 1. As for GTA welding, phase transformation temperatures change after laser welding, the changes being even larger for laser welds. These results indicate that certain post weld heat treatment may be required to recover the initial transformation behaviour. Such information is still lacking, but it should be noticed that the post heating temperature is important.

At least to some extent, the loss of initial properties of NiTi alloys following welding, can be reduced or minimized through the so called additive laser welding (Zhao et al 2008; Zhao et al, 2010). Ce was fed by pre-placement of a foil (TiNi with 2 at% Ce) between the two thin plates of NiTi. Nb was supplied through assembling NiTi to a specimen of NiTi with 9 at% Nb. The resulting effect of these additions after laser welding is to refine the solidification structure. Without Ce or Nb additions, the solidification structure is typically columnar grains growing from the fusion line towards the weld centre line, Fig. 10a. Growth of crystals will always proceed parallel to the steepest temperature gradient in the melt; i.e., perpendicular to the isotherms. Such crystals will quickly outgrow those grains with less favourable orientation. This implies that the columnar grain morphology is dependent on

the weld pool geometry, which again is controlled by the welding power, welding speed and the base metal thermal properties. In a laser weld, this may give almost a straight solidification line through the entire weld thickness. Since this area will be the last to solidify, it may contain most impurities, and hence, represent the weakest point. When adding Ce or Nb, this solidification pattern is broken, and the grains are equiaxed, Fig. 10b and c. This effect results in grain refinement since the growth of columnar grains is prevented. The consequence is an improvement of the stress-strain behaviour, as clearly evidenced in Fig. 11. Nb gave around 30% increases in strength, i.e., from 400 to 530 MPa fracture strength, and a rise in the strain at fracture beyond 40%. Ce was even more powerful and gave a strength increase twice as that found for the reference weld, and a strain at fracture of more than 200% better. For Ce, the mechanism seems to be related to formation of Ce oxides, which may act as nucleation sites in solidification, which means that the grain size is controlled by the volume fraction of the small oxide particles. For Nb, the mechanism is different. The second phase was identified as β-Nb, and solidifies at lower temperature (towards the completion of solidification). Thus, they will not act as nucleation sites, but rather prevent the growth of columnar NiTi grains.

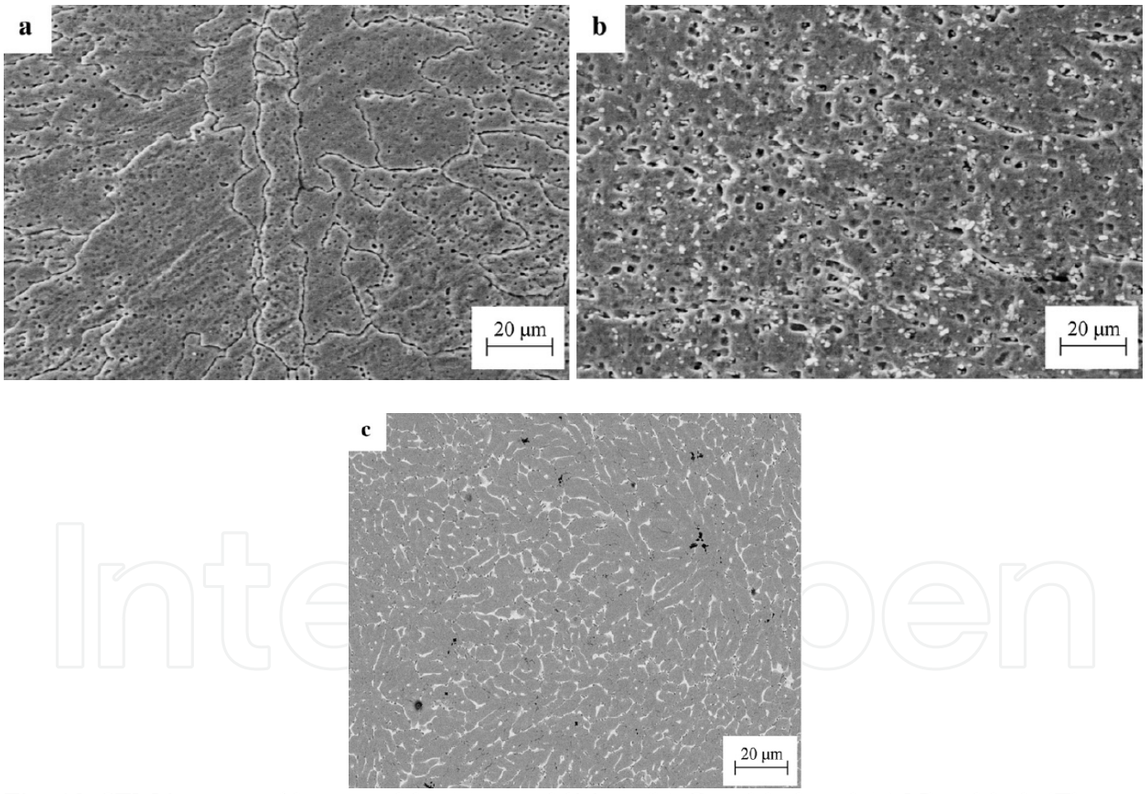


Fig. 10. SEM images of laser welds; (a) no additive, (b) Ce added and (c) Nb added. (Zhao et al, 2008).

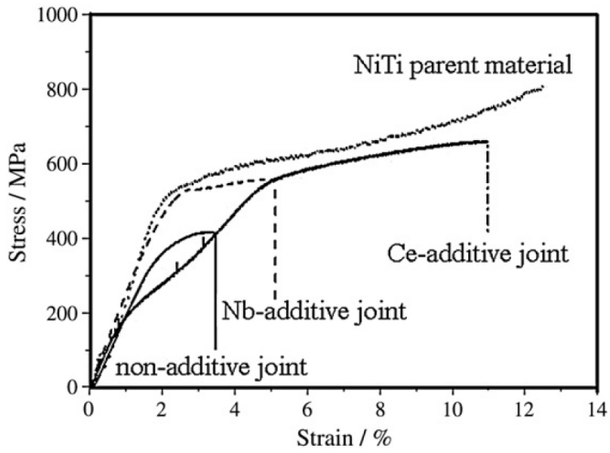


Fig. 11. Tensile stress-strain curve of NiTi before (full line) and after laser welding (dotted line). (Zhao et al, 2010).

Laser beam welding is promising in welding NiTi to stainless steel (Wang, 1997; Hall, 2003). As also observed in arc welding (van der Eijk et al, 2003 & 2004b), the stainless steel side is the one most exposed to reactions as expressed by a wider transition zone, Fig. 12. In Fig. 12a, epitaxial solidification is seen by the grains growing from the NiTi side into the weld metal.

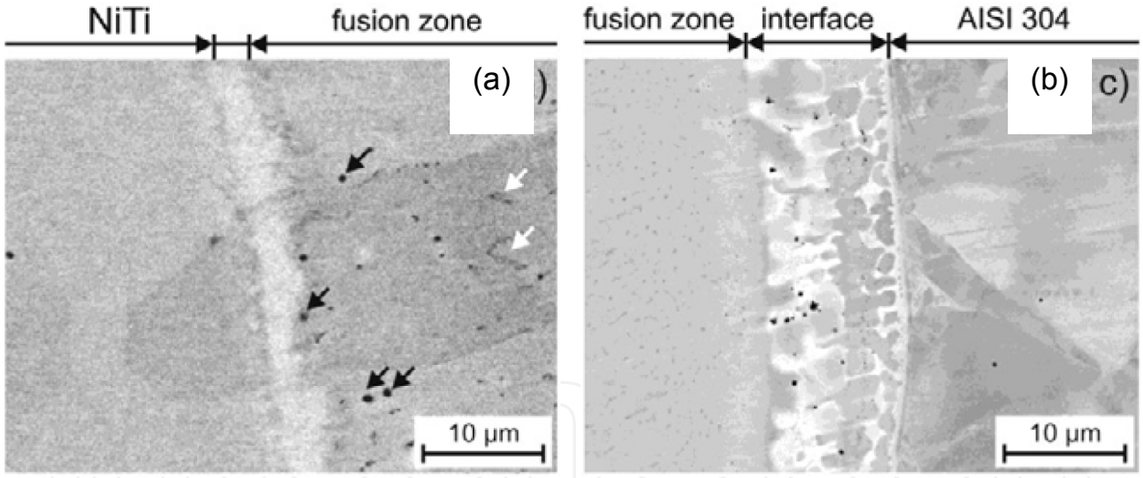


Fig. 12. SEM micrographs of NiTi-AISI 304 joint (Gugel & Theisen, 2009). (a) Interface between NiTi and fused zone, (b) interface between AISI 304 and fused zone.

The black and white arrows point out some precipitates in the weld metal. Since there is primary dendritic solidification of NiTi, these particles tend to precipitate in the interdendritic regions, being the last to solidify. An overview of the grain size distribution is illustrated in Fig. 13. The NiTi base metal consists of small grains of 30µm, while the HAZ contained smaller grains of 20 µm (Gugel & Theisen, 2009). On both sides of the weld, it is seen that the grains are nucleated at the respective fusion lines and grow inward towards the weld centre line (largest temperature gradient). A corresponding mapping of phases was also performed, and the map of the AISI 304/weld metal side is shown in Fig. 14. The

dominating phase is Fe_2Ti. According to the authors, the green phase in the stainless steel side has a bcc lattice, and is probably δ-ferrite due to ferritic solidification of laser welded austenitic stainless steel. Further development of laser welding with systematic variations in the welding parameters is needed, and the effects on weld properties should be clarified.

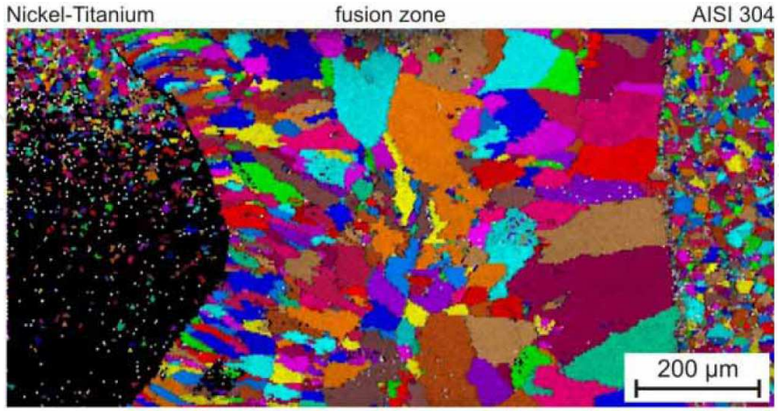


Fig. 13. Grain distribution mapping by EBSD (Gugel & Theisen, 2009).

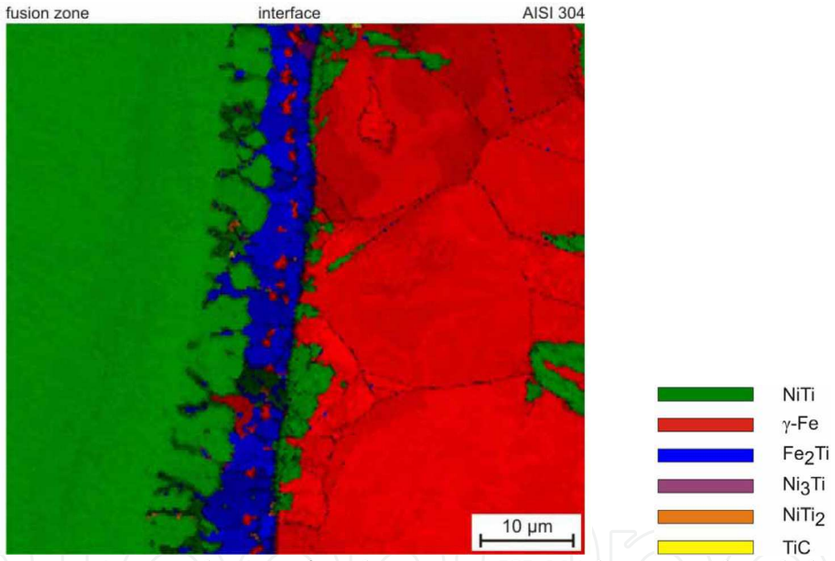


Fig. 14. Phase mapping on the interface between AISI 304 base metal and the fused zone (Gugel & Theisen, 2009).

In addition to stainless steel, laser welding (CO_2 gas laser) has been applied to joining of NiTi to the Ni-based alloy Inconel 625 and the Ni-Cu alloy Monel 400 (Tuissi et al, 2003). As found for stainless steel, extensive reactions take place at the Inconel and Monel sides of the welds. The welds gave poor strength and ductility due to transversal cracks in the as welded state. Such cracks are probably originating from welding residual stresses, in addition to the thermal expansion mismatch present. It is therefore necessary to change the chemical composition of the fused metal to reduce the cracking susceptibility. This can be done by simply adding a wire, powder or an interlayer to the fused metal during welding. Further work should be done to improve the properties of such dissimilar material joints for verification.

6. Brazing

In brazing processes, the base metals do not melt, and certain high temperature metallurgical phenomena can be avoided. These may consist of high temperature oxidation, elemental segregation and grain growth, which all may reduce the initial properties of SMA. However, even in brazing reactions will take place between the base metals and the filler alloy. Vacuum atmosphere is recommended, and the use of filler alloys containing active elements may be an advantage. An example is Ti, as indicated in Table 2 below. The table contains a survey of brazing alloys employed in this section, and AgCu alloys are the basis for all of them. In few other investigations, the use of Au and Au-based (Shiue & Wu, 2006a) or Nb (Grummon et al, 2006) filler alloys have been reported.

Alloy	Composition					Melting range, °C
	Ag	Cu	Zn	Sn	Ti	
AgCu (eutectic)	71.9	28.1	-	-	-	779
AgCuZnSn I	52	22	18	8	-	590-635
AgCuZnSn II	50-68	10-30	12-20	0-10	-	640-730
AgCuTi I	70.5	26.5	-	-	3	780-805
AgCuTi II [1]	63	35.25	-	-	1.75	780-815
AgCuTi III [2]	68.8	26.7	-	-	4.5	830-850
AgTi	96	-	-	-	4	970

[1] Cusil-ABA® [2] Ticusil®

Table 2. Brazing alloys.

As for welding, there are numerous different brazing processes, usually named after the heating method, i.e., torch, furnace, induction, dip and ultrasonic brazing, and others. For SMA in general, and NiTi particular, the alloy is quite reactive with oxygen, carbon, nitrogen and hydrogen, which set requirements to the brazing atmosphere. Thus, vacuum conditions may be preferable. To the author's knowledge, the effect of furnace pressure level on joint quality is not reported. However, brazing in 10^{-3} Pa pressure with eutectic Ag-Cu filler metal (72wt% Ag, melting temperature of 779°C) may give quite good strength and ductility, but is dependent on the overlap length. This point is shown in Fig. 15a. A considerable enhancement of strength is achieved when the overlap length is increased from 1 to 4 mm. The brazed specimen with 1 and 2 mm overlap fails at a load of 360 and 600 N, respectively, while the 4 mm overlap sample fractured at 980 N (about 820 MPa). In Fig. 15b, the recovery strain is plotted versus the total strain. Below 4% total strain (or 4% recovery strain), there is a linear 1:1 relation between the two strains, indicating 100% recovery. Beyond 4% strain, the recovery strain deviates from the 1:1 relationship with the total strain, approaching a plateau at ~ 7% for a total strain level of 10%. Obviously, a permanent loss of recovery is found.

In order to achieve a strong bond, there must be some chemical reaction following the diffusion processes between the base metals and the filler. Such reactions are the basis for brazing and cause formation of a reaction layer between the base metal and the brazing alloy. An example of resulting microstructure is shown in Fig. 16, clearly resembling the typical eutectic microstructure of Ag-Cu brazing alloys, consisting of white Ag and grey Cu

rods. Note also the formation of reaction layer at the interface between the base metal and brazing alloy. The authors suggested this phase to be of the type XTi_2 (Zhao et al, 2009), where X=Ni+Ag+Cu. According to the binary phase diagram, Ni and Cu have full mutual solubility at the brazing temperature, while at low temperature (354°C), a spinodal decomposition causes phase separation into α_1 and α_2. Since there is no thermodynamic barrier to the reaction inside of the spinodal region, the decomposition is determined solely by diffusion. In the Ag-Cu and Ag-Ni binary phase diagrams, there are no intermetallic compounds formed. Moreover, there is limited solid solubility of Ni in Ag in the Ag-Ni system. By contrast, all elements (Ag, Cu, Ni) form numerous intermetallic compounds with Ti, Table 3. Therefore, the formation of intermetallics at the interface between the base metal and the brazing alloy is expected.

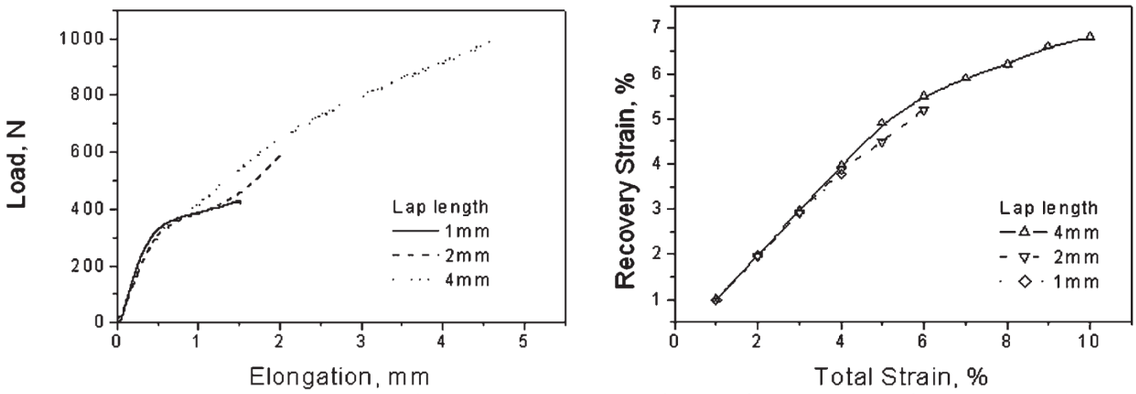


Fig. 15. Stress-strain curves and recovery strain of NiTi/NiTi joints for various brazed overlap length; brazed at 900°C for 5 min (Zhao et al, 2009).

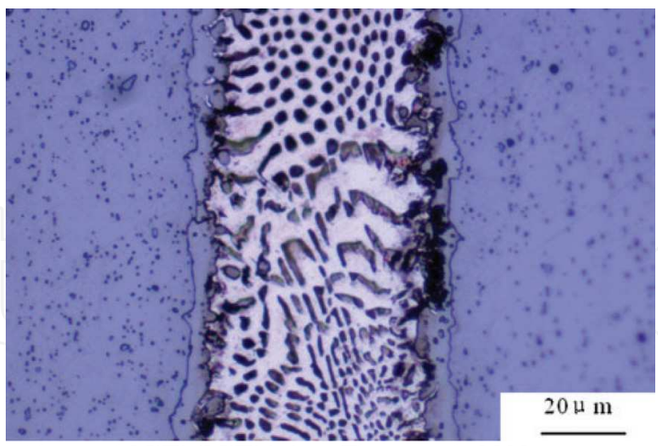


Fig. 16. Micrograph of brazed NiTi/NiTi joint (Zhao et al, 2009).

Element	**Compound**					
Ag	AgTi	$AgTi_2$				
Cu	Cu_4Ti	Cu_2Ti	Cu_3Ti_2	Cu_4Ti_3	CuTi	$CuTi_2$
Ni	Ni_3Ti	NiTi	$NiTi_2$			

Table 3. Intermetallic compounds in Ti_xX_y (X = Ag, Cu, Ni). (ASM Handbook, 1992)

Similar results have been found in both infrared (Shiue & Wu, 2006b) and microwave brazing (Chiu et al, 2005; van der Eijk et al, 2008). Ni may substitute Cu in XTi_2, which means that the concentration of Ni and Ti within the phase may vary quite significantly, i.e., $Ni_{67-x}Cu_xTi_{33}$. In addition, a Cu-Ti-Ni phase with some Ag was found. Finally, an Ag-rich phase will form in the brazing alloy. In summary, it is evident from experimental observations that Ag does not react with the Ni-Ti base metal. On the other hand, Cu and Ti in the brazing alloy react extensively with Ni-Ti to form XTi_2 (X = Cu+Ni, plus possibly some Ag) or Cu-Ni-Ti phases.

Using data from Villars et al (1995) and the liquidus projection of the Ag-Cu-Ti phase diagram contained in Fig. 17, the following reactions are possible in solidification of the molten Ag-Cu-Ti brazing alloy (point *A* in the figure; reference is made to the discussion by Shiue & Wu, 2006b):

At 808°C: $L + Cu_3Ti_2 \rightarrow (Ag) + Cu_4Ti$ (1)

At 783°C: $L + Cu_4Ti \rightarrow (Ag) + (Cu)$ (2)

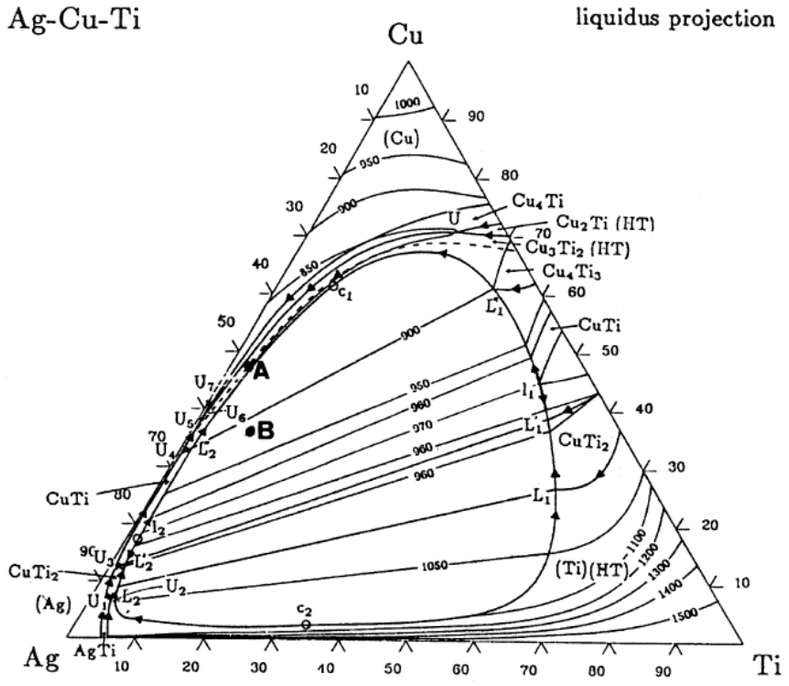
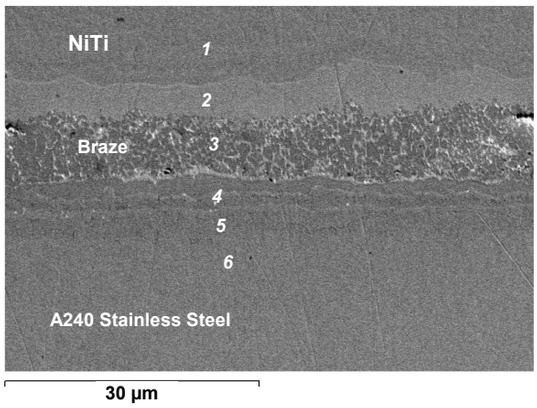


Fig. 17. Liquidus projection in ternary Ag-Cu-Ti phase diagram (Villars et al, 1995). Letters A and B refer to the brazing alloy compositions used by the authors.

On this background, the authors concluded that the microstructure of the solidified brazing alloy mainly comprised of Ag-rich and Cu-rich phases.

While NiTi has limited solubility of Ag, a certain solubility of Cu exists. Thus, both CuNiTi and (Cu,Ni)Ti may form in the Cu-Ni-Ti ternary system (Yang et al, 2004). It is also stated that, while the CuNiTi phase deteriorates the shape recovery ability, the (Cu,Ni)Ti phase preserves the shape memory behaviour (Mercier & Melton, 1979; Bricknell et al, 1979; Bricknell & Melton, 1980).

When brazing Ni-Ti to other metal, the situation is much more complex, depending on the actual metal. The Ni-based superalloy Hastelloy C-276[b] and austenitic stainless steel[c] results in extensive inter-diffusion of elements. An example is contained in Fig. 18 for NiTi/stainless steel joint. On the NiTi side of the joint there is formed a (Cu,Ni)Ti phase, while a Fe-Cr rich phase is formed on the steel side. Since reaction layer formation is a diffusion controlled process, the temperature and time used in brazing will indeed be important, in addition to the brazing alloy selection.



Position	Ni	Ti	Fe	Cr	Cu	Ag	Phase
1	57.3	42.7	-	-	-	-	NiTi base metal
2	28.3	26.8	2.2	-	42.7	-	(Cu,Ni)Ti
3	13.3	32.6	13.0	-	40.3	0.8	(Cu,Ni,Fe)Ti
4	6.0	3.7	59.9	30.4	-	-	FeCr-rich phase with some Ni,Ti
5	10.4	1.0	63.8	24.8	-	-	Stainless steel base metal
6	13.1	-	66.4	20.5	-	-	Stainless steel base metal

Fig. 18. SEM secondary electron image of the NiTi-stainless steel joint, brazed with Ag-Cu-Ti at 925 ^{o}C (van der Eijk et al, 2008).

In laser brazing, using the AgCuZnSn II brazing alloy in Table 2, low heat input gave low tensile strength of 190-210 MPa (Qiu et al, 2006). The strength was raised to 320-360 MPa when higher heat input was used. Keeping in mind that the initial base metal tensile strength was beyond 1100 MPa for both the NiTi alloy and the stainless steel, considerable loss in strength is caused by the brazing process. Similar findings were reported with the brazing alloy AgCuZnSn I in Table 2 (Li et al, 2006). As found in Fig. 18, interdiffusion and formation of numerous compounds take place, even more extensive than in the figure. Ag, Cu, Zn and Sn diffuse from the filler metal into both the base metals NiTi and stainless steel, while Ti and Ni from the NiTi side, and Fe, Cr and Ni from the steel side diffuse into the filler metal. The reaction layers on both sides will depend on the brazing parameters.

[b] Hastelloy C-276® contains 55wt% Ni, 14.5-16.5wr% Cr, 15-17wt% Mo, 4-7wt% Fe and 3-4.5wt% W.
[c] Containing 18-20wt% Cr, 8-10.5wt% Ni, 2wt% Mn, 1wt% Si and 0.08wt% C.

7. Adhesive bonding

Available information on adhesive bonding of NiTi is very limited. This is a bit surprising, since adhesive bonding may have limited negative influence on the initial base metal properties. Adhesives such as cyanoacrylates, epoxies, etc, can be used, when knowing the degradation susceptibility of them in different service environments. Adhesive bonding requires some surface pre-treatment to enhance the adhesion between the adhesive and the SMA base metal (Rossi et al, 2008). Such surface treatments have been applied in SMA composites consisting of NiTi wires embedded in a polymer matrix. Several surface treatment techniques have been reported, such as acid etching, polymer coating and sandblasting techniques (Paine et al, 1992) to improve the adhesion of NiTi wires to epoxy matrix. The authors concluded that sandblasting was the most efficient technique. The debonding strength was found to increase by 70%. As much as 180% improvement in debonding strength has been achieved in a similar examination (Jonnalagadda et al, 1997). Silane-coupling agents gave also 100% improvement in the adhesion strength (Smith et al, 2004). Various chemical etchants to treat NiTi fibres have been tested, but without the same strength enhancement; only 3-18% improvement was obtained (Jang & Kishi, 2005).

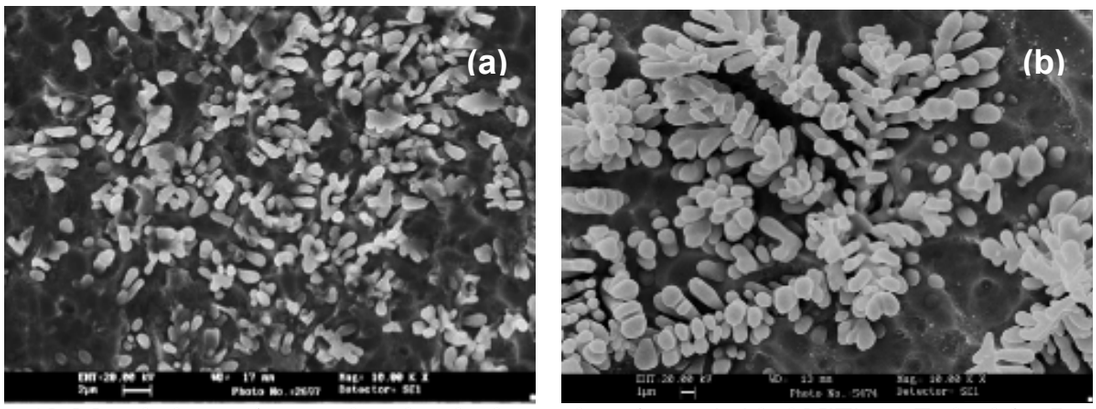


Fig. 19. Morphology of ground and etched samples of gas nitrided NiTi; (a) Etched for 5 min, and (b) etched for 30 min (Man & Zhao, 2006).

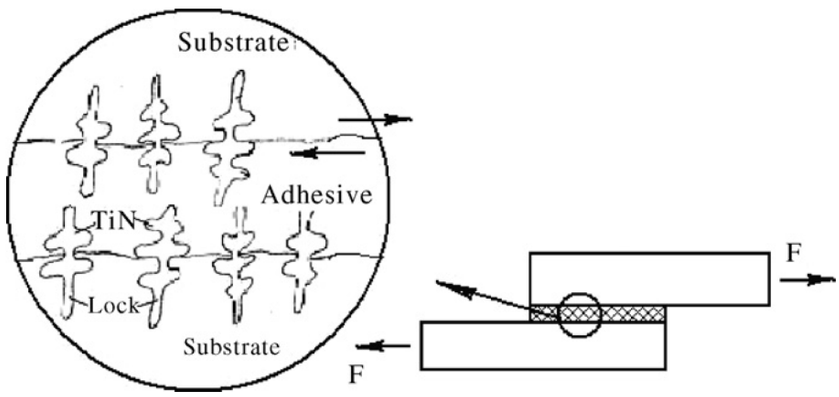


Fig. 20. Adhesive bonding (schematic) of lap joint and corresponding shear testing (Man & Zhao, 2006).

More promising then is surface coating by gas nitriding which provide hard TiN dendrites protruding from the NiTi intermetallic matrix (Cui et al, 2003; Man et al, 2005). This dendritic network, which occurs by chemical etching after the gas nitriding, gives very large increase in surface area, Fig. 19. This surface network strengthens the adhesion between the NiTi alloy and the adhesive. The concept is illustrated in Fig. 20 together with the test set-up for overlap bonding followed by shear testing. The shear test results shown in Fig. 21 reveal a considerable rise in shear strength compared with sandblasting and etching treatment. The strength level is raised from 8 to 15-20 MPa, depending on the etching time. Maximum strength of 20 MPa is found for an etching time of 30 min. These variations with etching time are closely linked to the surface morphology, which is indicated in Fig. 22.

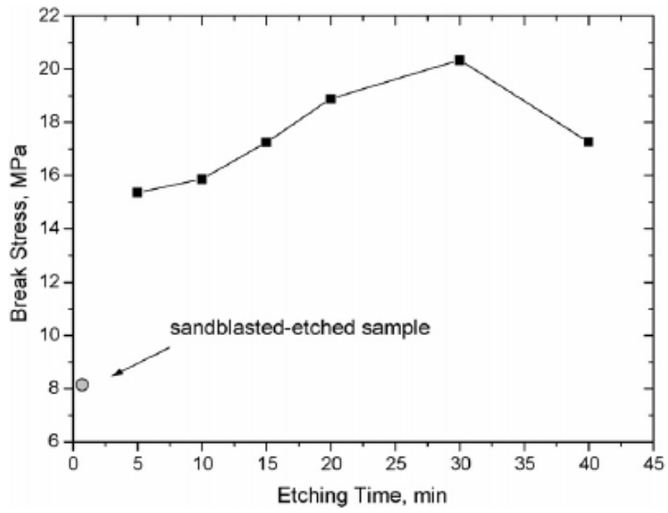


Fig. 21. Effect of etching time on lap joint shear strength (Man & Zhao, 2006).

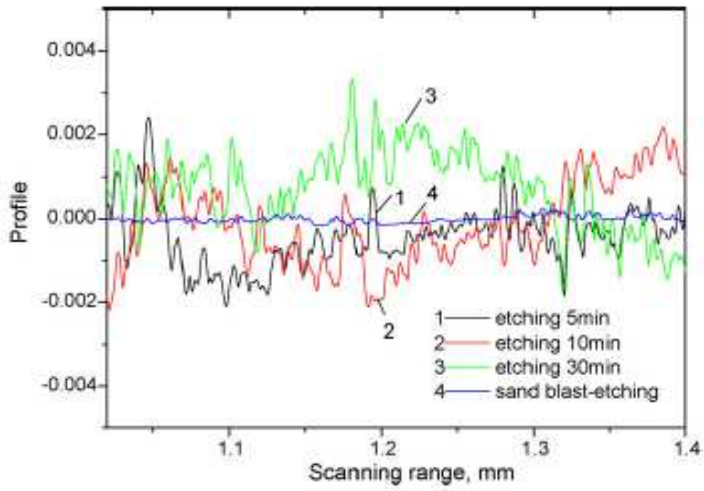


Fig. 22. Surface roughness of treated NiT (Man & Zhao, 2006).

Recent findings (Sadmezhaad et al, 2009) have also indicated that oxidation may give substantial improvement to the adhesion between NiTi and polymers, Fig. 23. Again, the

adhesion strength seems to be proportional with the surface area, which is dramatically increased by the surface treatment change from type P, via types E and AO, to type O techniques.

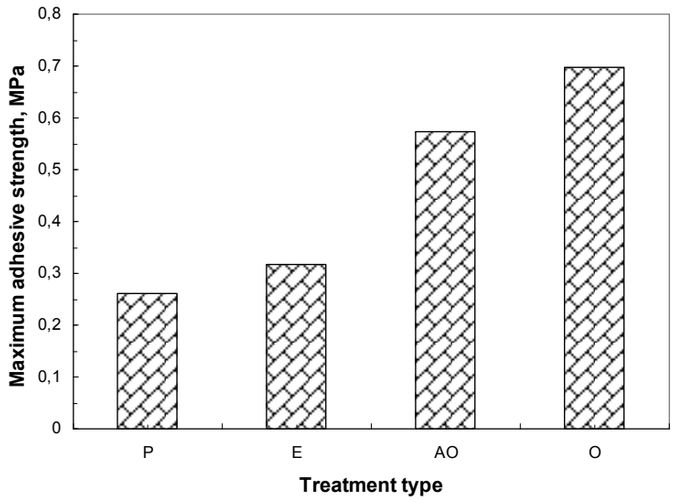


Fig. 23. Comparison of adhesive strength for different surface treatment techniques Sadmezhaad et al, 2009). (P) Straight-annealed, scraped, cleansed and washed, (E) straight-annealed, scraped, cleansed and etched, (AO) abraded and straight-annealed, and (O) straight-annealed.

8. Other techniques

Friction welding is normally an excellent process alternative when joining round bars since this joint fit-up satisfies the symmetry requirements in conventional and inertia friction welding. The first attempt to weld NiTi by friction was performed two decades ago (Shinoda et al, 1991). Although the base metal does not melt, there is substantial change in the phase transformation temperatures and loss in strength. Subsequent heat treatment at 500°C enhanced the as-welded properties to approach the same level as the base metal. This early work has not been followed up, and more information on the effects of process parameters is needed. Friction welding produces an upset collar, which needs to be removed by machining, another challenging issue.
NiTi alloys have also been friction welded to austenitic stainless steel with and without a Ni interlayer (Fukumoto et al, 2010). Without the use of Ni interlayer, a large amount of brittle Fe_2Ti intermetallic compound was formed at the weld interface. The formation of this brittle compound led to degradation of the joint strength. Use of Ni interlayer changed the microstructures at the weld interface and improved the joint strength. Fracture occurred at the interface between Ni and NiTi. The interface between Ni and NiTi was free from Fe_2Ti and consisted of mainly Ni_3Ti and NiTi.

Friction stir welding (Thomas et al, 1991) (FSW) is a special variant of friction welding used for applications where the original metal characteristics must remain unchanged as far as possible. In FSW, a cylindrical-shouldered tool, with a profiled threaded/unthreaded pin is

rotated at a constant speed and fed at a constant traverse rate into the joint line between two pieces of sheet or plate material, which are butted together. Usually, the parts have to be clamped rigidly onto a backing bar in a manner that prevents the abutting joint faces from being forced apart. There are many challenges, of which the tool design and material is of great significance to the welding performance and weld quality. Tool wear may represent a huge threat against industry applications of the process. FSW has been applied to join NiTi (6.35 mm thick plates), using polycrystalline cubic boron nitride and tungsten-rhenium tool materials London et al, 2005). Similar to that measured after arc welding and beam welding, there is a change in the phase transformation temperature after welding, Fig. 24.

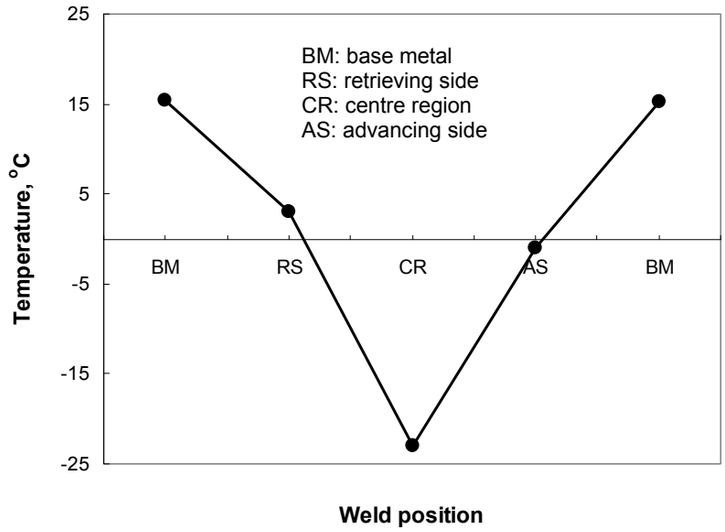


Fig. 24. Variation in austenite finish temperature across a friction stir weld (London et al, 2005).

Resistance upset butt welding has been applied for NiTi wires. Resistance welding is based upon use of electrical current and mechanical pressure to produce a weld between two parts. Welding electrodes lead the current to the two parts that are squeezed together and subsequently welded. Usually, the weld cycle must first generate adequate heat to melt a small volume, with subsequent cooling under the influence of pressure until a weld is formed with sufficient strength to keep the parts together. In conventional resistance spot and seam welding, the current density and the pressure are kept sufficiently high to form a weld, but not too high such that the material is squeezed out from the weld zone. However, in upset welding, there is an upset collar formed which usually needs to be removed by machining after welding (Nishikawa et al, 1982). The authors reported strength reduction, e.g., the tensile strength of the welds was about 80% of that of the base metal. Unfortunately, there is no follow up of this early work on resistance welding.

Explosion welding has been carried out related to manufacture of NiTi laminates. The principle is shown in Fig. 22. The joint is formed by the high velocity impact of the work pieces as a result of controlled detonation. The method consists of three main materials: (i) the base metal, (ii) the flyer, and (iii) the explosive. The main parameters in welding are the

collision speed, collision angle, and the flyer speed. The interface or weld line between the base metal and the flyer is usually wavy. Apparently, this is not the case for NiTi/NiTi joint shown in Fig. 23. By this technique, NiTi can be welded to itself and to other metals. However, it is reasonable to suggest that the process will have geometric symmetry limitations, imposing restrictions to the component design.

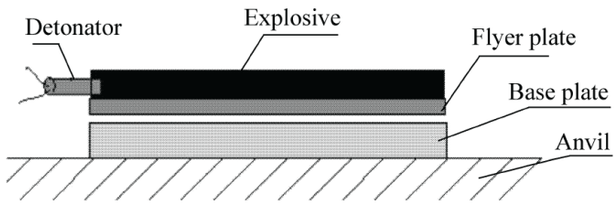


Fig. 25. Explosion welding principles.

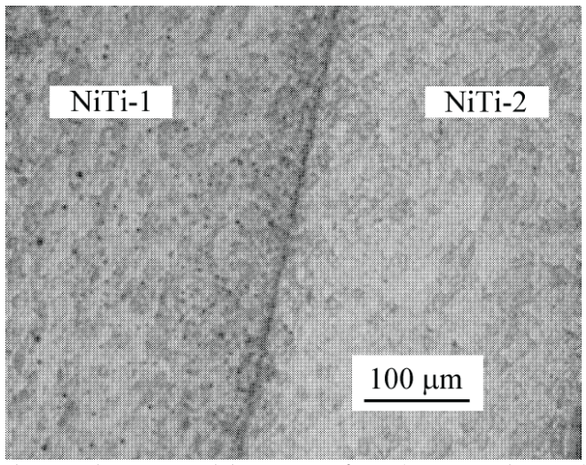


Fig. 26. Micrograph of the explosion welding interface (Yan et al, 2007).

Transient liquid phase (TLP) diffusion bonding is another possible route reported for both CuAlZn (Gomez de Salazar et al, 1997) and NiTi alloys (Kejanli et al, 2009). Diffusion bonding is a process that combines the use of temperature and pressure. The temperature range is typically 50-80% of the base metal melting temperature. The pressure is applied to provide good contact and to cause plastic deformation of surface asperities. The CuAlZn alloy was subjected to TLP diffusion bonding with an Ag interlayer. Ductile interlayers are typically used when joining dissimilar materials to accommodate strains due to different thermal expansions. The Ag interlayer was selected since Ag-Cu alloys are used as filler metals in brazing. The authors showed by their experiments that, when using their optimum bonding procedure, the shape recovery reached a value of 91% of the base metal. Also in TLP diffusion bonding of NiTi, an interlayer was used. Cu was selected, and assists in providing the transient liquid phase (low melting eutectic phase).

Soldering should also be a feasible technique for joining NiTi to itself or to other metals. An example is an early work with AgPd and AgPdGa solder alloys (Segoshi et al, 1990). Other examples are the SnAg and AuSn solders with low melting temperatures between 200 and 300°C (www.indium.com). Since SMA may be quite reluctant to wetting by solders, they

may be surface treated by e.g., nickel to provide a less reactive surface (easier to wet). Alternatively, a reactive flux must be used to remove the surface oxide present. Such flux may be a non-aqueous molten salt formulated on eutectic mixtures of KOH (potassium hydroxide), NaOH (sodium hydroxide) and LiOH (lithium hydroxide), with melting temperatures in a range from about 170 to about 226° C) (Nanis, 2005). The use of an aggressive flux permits joining of SMA to other metals (e.g., stainless steel). Soldering kits are also available today, containing both the required flux and solder alloy.

It is worth to mention that shape memory alloys like NiTi is also added as reinforcements in solder alloys to improve their stress-strain behaviour. Moreover, shape memory alloys are used as couplings themselves in e.g., tube joining. Bolted connections are also made in memory metals. Such use of these alloys is outside the scope of the present report.

9. Summary and concluding remarks

In the present report, the joining of shape memory alloys to themselves or to other metals is discussed. The joining processes included are arc welding, beam welding, brazing, adhesive bonding and some other techniques like friction welding, resistance welding, explosive welding, transient liquid phase diffusion bonding and soldering.

Welding of SMA by arc welding or beam welding processes is possible but tends to produce brittle joints. Brittleness can be reduced by stress relieving, but degradation of the shape memory effect may occur due to the high temperatures that are required. Welding should also be carried under inert gases to prevent passive oxide build-up. Welding is seen to change the phase transformation temperatures, which may reduce the application window. Post welding training cycles may enhance the as welded shape memory effect and superelasticity. Laser welding tend to give narrow welds, and may thus be preferable to arc welding due to possible finer microstructure and lower thermal stresses and strains left from the welding cycle. Welding of SMA to other metals may be challenging due to the extensive formation of intermetallic compounds. These tend to be very brittle. In such cases, it may be required to use additives that prevent such formation, but very little information is available. Such information would be of great interest to expand the application of SMA-metal couplings.

Several brazing processes have been studied, including infrared furnace, laser heating and microwave heating. The main advantage of brazing is that the base metals do not melt, and that there are commercially available brazing alloys, mainly based on Ag-Cu-mixtures. Like welding, certain reduction of the initial base metal properties should be expected. Formation of intermetallic compounds at the interface between the base metal and brazing alloy will take place. This is a necessity to achieve strong bonds, but may also be negative due to the brittle nature of many of these phases. The XTi_2 (where X = Cu, Ni and/or Ag) phase is regarded to be very brittle. Brazing of SMA to other metals will give complex interdiffusion across the joint with significant reaction layer formation. The use of proper, ductile interlayer may be good choice to prevent the excessive diffusion and to accommodate thermal strains due to mismatch in thermal expansion.

Like welding, passive oxide build-up can be problematic when soldering nickel-titanium alloys. While being difficult, it can be done using SnAg or AuSn solders with an aggressive flux. Alternatively, plating with nickel or gold prior to soldering can result in good solder joints. The melting temperature of these solders is low, between 200 and 300ºC.
Transient liquid phase diffusion bonding utilizes low melting eutectics, and the process combines temperature and pressure. This eutectic is achieved by using interlayers that assist in the formation of the low melting eutectic phase. Shape recovery up to 91% has been reported.

Friction welding, both conventional and friction stir welding, has been performed. These are solid state processes, but the heavy deformation of the weld zone may cause degradation in the properties such as superelasticity, shape memory and phase transformation temperatures. Resistance welding was tested in the early stages of SMA development. The method gave promising tensile results, but has not been fully explored.

Explosion welding has been applied in NiTi-NiTi laminate production. The technique is also feasible in joining or coating NiTi to other metals, although some limitations will be present.
Shape memory alloys can be joined by adhesive bonding, but surface pre-treatment is often required to enhance the bonding area. Adhesives such as cyanoacrylates, epoxies, etc, can be used, when knowing the degradation susceptibility of them in different service environments. Mechanical methods such as crimping and swaging have also been successful. The shape memory effect itself can be used and has been employed commercially in couplings.

As envisaged in the report, a great variety of joining processes has been applied to shape memory alloys. However, to some extent, there is still a lack of systematic studies on the effects of joining parameters. There is still some way to go concerning process and performance optimization, and hence, there is certainly a need for keeping the focus on joining also in the years to come.

Finally, it should be noticed that, although degradation of properties occurs in most joining processes using heat, this deterioration may take place locally. The significance of local strength or ductility changes in a component is not very clear, and there is a need for finite element modelling to simulate the impact on the component structural integrity. Moreover, with brittle materials or local brittle constituents, formation of microcracks has been observed in joining, especially when joining NiTi to other materials. The significance of such microcracks should be assessed by fracture mechanics. Some studies have been carried out (Chen at al, 2005; Daymond et al, 2007; Wang, 2007; Maletta et al, 2009), but the topic deserves more attention in future work.

10. References

ASM Handbook: Alloy Phase Diagrams, Vol.3, 1992, ASM International, Metals Park, Ohio, USA.

Bricknell, R.H., Melton, K.N. & Mercier O. (1979). The structure of NiTiCu shape memory alloys. *Metal Trans.*, 10A, 693-697.

Bricknell, R.H. & Melton, K.N. (1980). Thin foil electron microscope observations on NiTiCu shape memory alloys. *Met. Trans.*, 11A, 1541-1546.

Buehler, W.J. & Wiley, R.C. (1965). Nickel base alloys. US Patent 3174851, March 23.

Chen, J.H., Sun, W. & Wang, G.Z. (2005). Investigation on the fracture behaviour of shape memory alloy NiTi. *Metall. Mater. Trans.*, 36A, 941-955.

Chiu, K.Y., Cheng, F.T., Man, H.C. (2005). A preliminary study of cladding steel with NiTi by microwave –assisted brazing. *Mater. Sci. Eng.*, A 407, 273-281.

Cui, Z.D., Man, H.C. & Yang X.J. (2003). Characterization of the laser gas nitrided surface of NiTi SMA. *Appl. Surf. Sci.*, 208-209, 388-309.

Daymond, M.R., Young, M.L., Almer, J.D. & Dunand, D.C. (2007). Strain and texture evolution during mechanical loading of a crack tip in martensitic shape-memory NiTi. *Acta Mater.*, 55, 3929-3942.

Dong, Z.Z., Sawaguchi, T., Kajiwara, S., Kikuchi, T., Kim, S.H. & Lee, G.C. (2006). Microstructure change and shape memory characteristics in welded Fe-28Mn-6Si-5Cr-0.53Nb-0.06C alloy. *Mater. Sci. Eng.*, A 438-440, 800-803.

Eijk, C. van der, Fostervoll, H., Sallom, Z. & Akselsen, O.M. (2003). Plasma Welding of NiTi to NiTi, Stainless Steel and Hastelloy C276", *Int. Conf. Joining of Specialty Materials VI Program*, ASM Materials Solutions Conf. & Exposition, Oct. 13-15, Pittsburgh, PA, USA.

Eijk, C. van der, Zhang, Z. & Akselsen, O.M. (2004a). Seismic Dampers Based on Shape Memory Alloys: Metallurgical Background and Modelling. *Proc. 3rd European Conf. on Structural Control*, 3ECSC, July 12-15, Vienna Univ. of Technol., Vienna, Austria.

Eijk, C. van der, Fostervoll, H., Sallom, Z. & Akselsen, O.M. (2004b). Plasma Welding of NiTi to NiTi, Stainless Steel and Hastelloy C276. *Proc. Int. Conf. Advanced Metallic Materials and Their Joining*, October 25-27, Bratislava, Slovakia. International Institute of Welding.

Eijk C. van der, Sallom, Z.K. & Akselsen, O.M. (2008). Microwave brazing of NiTi shape memory alloy with Ag-Ti and Ag-Cu-Ti alloys. *Scripta Mater.*, 58, 779-781.

Falvo, A., Furgiulele, F.M. & Maletta, C. (2005). Laser welding of a NiTi alloy: Mechanical and shape memory behaviour. *Mater. Sci. Eng.*, A 412, 235-240.

Falvo, A., Furgiulele, F M. & Maletta, C. (2008). Functional behaviour of a Ni-Ti welded joint: Two-way shape memory effect. *Mater. Sci. Eng.*, A 481-482, 647-650.

Fukumoto, S., Inoue, T., Mizuno, S., Okita, K., Tomita, T. & Yamamoto, A. (2010). Friction welding of TiNi alloy to stainless steel using Ni interlayer. *Sci. Technol. Weld. Join.*; 15, 124-130.

Gomez de Salazar, J.M., Mendez., F.J., Urena, A., Guilemany, J.M. & Mellor, B.G. Transient liquid phase (TLP) diffusion bonding of a copper based shape memory alloy using silver as interlayer. *Scripta Mater.*, 37, 861-867.

Grummon, D.S., Shaw, J.A. & Foltz, J. (2006). Fabrication of cellular shape memory alloy materials by reactive eutectic brazing using niobium. *Mater. Sci. Eng.*, A 438-440, 1113-1118.

Gugel, H., Schuermann, A. & Theisen, W. Laser welding of NiTi wires. (2008). *Mater. Sci. Eng.*, A 481-482, 668-671.

Gugel, H. & Theisen, W. (2009). Microstructural investigation of laser welded dissimilar nickel-titanium-steel joints. *Proc. 8th European Symposium on Martensitic Transformations* (ESOMAT), Paper 05009, September 7-11, Prague, Czech Republic.

Haas, T. & Schüssler, A. (1999). Welding and joining of TiNi shape memory alloys: Engineering aspects and medical applications. *Proc. 1st European Conf. Shape Memory and Superelastic Technologies* (SMST '99), pp.1-11, Sept. 5-9, Antwerpen, Belgium.

Hall, P.C. (2003). Laser welding Nitinol to stainless steel. *Proc. Int. Conf. Shape Memory and Superelastic Technologies*, pp.219-228, Pacific Grove, CA, USA.

Hosoda, H., Hanada, S., Inoue, K., Fukui, T., Mishima, Y. & Suzuki, T. (1998). Martensite Transformation Temperatures and Mechanical Properties of Ternary NiTi Alloys with Offstoichiometric Compositions. *Intermetallics*, 6, 291-301.

Hsu, Y.T., Wang, Y.R., Wu, S.K. & Chen, C. (2001). Effect of CO_2 Laser Welding on the Shape-Memory and Corrosion Characteristics of TiNi Alloys. *Metall. Mater. Trans.*, 32A, 569-576.

Ikai, A., Kimura, K. & Tobushi, H. (1999). TIG Welding and Shape Memory Effect of TiNi Shape Memory Alloy. *Jour. Int. Mat. Syst. Struc.*, 7, 646-655.

Jang, B.K. & Kishi, T. (2005). Adhesive strength between TiNi fibres embedded in CFRP composites. *Mater. Lett.*, 59, 1338-1341.

Janke, L., Czaderski, C., Motavalli, M. & Ruth, J. (2005). Applications of shape memory alloys in civil engineering structures – Overview, limits and new ideas. *Mater. Struct.*, 38, 578-592.

Jonnalagadda, K., Kline, G.E. & Sottos, N.R. (1997). Local displacements and load transfer in SMA composites. *Exp. Mech.*, 37, 78-85.

Khan, M.I., Panda, S.K., Zhou, Y. (2008). Effects of welding parameters on the mechanical performance of laser welded Nitinol. *Mater. Trans.*, 49, 2702-2708.

Kejanli, H., Taskin, M., Kolukisa, S. & Topuz, P. (2009). Transient liquid phase (tlp) diffusion bonding of $Ti_{45}Ni_{49}Cu_6$ P/M components using Cu interlayer. *Int. J. Adv. Manuf. Technol.*, 44, 695-699.

Li, M.G., Sun, D.Q., Qiu, X.M., Sun, D.X. & Yin, S.Q. (2006). Effects of laser brazing parameters on microstructure and properties of TiNi shape memory alloy and stainless steel joint. *Mater. Sci. Eng.*, A 424, 17-22.

London, B., Fino, J., Pelton, A.R. & Mahoney, M. (2005). Friction stir processing of Nitinol. In *Friction Stir Welding and Processing III*, Eds. K.V. Jata, M. W. Mahoney, R.S. Mishra, T.J. Lienert, TMS, Warrendale.

Maletta, C., Falvo, A., Furgiuele, F., Barbieri, G. & Brandizzi M. (2009). Fracture behaviour of nickel-titanium laser welded joints. *J. Mater. Eng. Perform.*, 18, 569-574.

Man, H.C., Zhao, NQ.. & Cui, Z.D. (2005). Surface morphology of a laser surface nitrided and etched Ti-6Al-4V alloy. *Surf. Coat. Technol.*, 192, 341-346.

Man, H.C. & Zhao, N.Q. (2006). Enhancing the adhesive bonding strength of NiTi shape memory alloys by laser gas nitriding and selective etching. *Appl. Surf. Sci.*, 253, 1595-2000.

Mercier, O. & Melton, K.N. (1997). The substitution of Cu for Ni in NiTi shape memory alloys. *Metal Trans.*, 10A, 387-389.

Miyazaki, S., Otsuka, K. & Suzuki, Y. (1981). Transformation pseudoelasticity and deformation behaviour in a Ti-50.6 at%Ni alloy. *Scripta Metall* , 15, 287-292.

Miyazaki, S., Ohmin, Y. & Otsuka K. (1982). Characteristics of deformation and transformation pseudoelasticity in Ti-Ni alloys. *J de Phys.*, 43, 255-260.

Miyazaki, S., Igo, Y. & Otsuka, K. (1986). Effect of thermal cyclic deformation on the pseudoelasticity characteristics of Ti-Ni alloys. *Acta Metall*, 34, 2045-2051.

Morgan, N B. (2004). Medical shape memory alloy applications – the market and its product. *Mater. Sci. Eng.*, A 378, 16-23.

Nanis L. (2005). Low-temperature flux for soldering nickel-titanium alloys and other metals. US Patent 6,953,146, Oct. 11.

Nishikawa, N., Tanaka, H., Kohda, M., Nagaura, T. & Watanabe, K. (1982). Behaviour of welded part of Ti-Ni shape memory alloys. *J. de Phys.*, 43, C4, C4-839 – C4-844.

Paine, J.S.N., Jones, W.M. & Rogers, C.A. (1992). Nitinol actuator to host composite interfacial adhesion in adaptive hybrid composites. *Proc. 33rd Structural Dynamics and Materials Conf.*, AIAA, pp.556-565.

Pfeifer, R., Herzog, D., Ostendorf, A., Meier, O., Haferkamp, H., Goesling, T., Muellller, C. & Hurschler, C. (2008) Laser Welding of Shape Memory Alloys for Medical Applications. *Proc. ICALEO*, Paper #M601.

Qiu, X.M., Li, M.G., Sun, D.Q. & Liu, W.H. (2006). Study on brazing of TiNi shape memory alloy with stainless steels. *J. Mater. Proc. Technol.*, 176, 8-12.

Rossi, S., Deflorian, F., Pegoretti, A., D'Orazio, D. & Gialanella, S. (2008). Chemical and mechanical treatments to improve the surface properties of shape memory alloy wires. *Surf. Coat. Technol.*, 202, 2214-2222.

Saadat, S., Salichs, J., Noori, M., Davoodi, H., Bar-on, I., Suxuki, Y. & Msuda A. (2002). An Overview of Vibration Seismic Applications of NiTi Shape Memory Alloy. *Smart Mater. Struct.*, 11, 218-224.

Sabur, T., Yoshida, M. & Nenno S. (1984). Deformation behaviour of shape memory Ti-Ni alloy crystals. *Scripta Metall. Mater.*, 18, 363-366.

Sadrnezhaad, S.K., Nermati, N.H. & Bagheri, R. (2009). Improved adhesion of NiTi wire to silicone matrix for smart composite medical applications. *Mater. Design*, 30, 3667-3672.

Schlossmacher, P., Haas, T. & Schüssler, A. (1994). Laser Welding of Ni-Ti Shape Memory Alloys. *Proc. 1st Int. Conf. Shape Memory and Superelastic Technologies*, pp.85-90, Pacific Grove, CA, USA.

Schlossmacher, P., Haas, T. & Schüssler, A. (1997a). Laser Welding of a Ni-rich TiNi Shape Memory Alloy: Pseudoelastic properties. *Proc. 2nd Int. Conf. Shape Memory and Superelastic Technologies*, pp.137-142, Pacific Grove, CA, USA.

Schlossmacher, P., Haas, T. & Schüssler, A. (1997b). Laser Welding of a Ni-rich TiNi Shape Memory Alloy: Mechanical behaviour. *J. Phys. IV*, 7, C-251 – C-256.

Segoshi, K., Okuda, T., Okamura, K. & Yoshida, M. (1990). Soldering material for spectacle frame and spectacle frame in which said soldering material is used. US Patent 4,976,529, Dec.11.

Shinoda, T., Tsuchiya, T. & Takahashi, H. (1991). Functional Characteristics of Friction Welded Near-Equiatomic TiNi Shape Memory Alloy. *Trans. Jap. Weld. Soc.*, 22, 30-36.

Shiue, R.H. & Wu, S.K. (2006a). Infrared brazing of $Ti_{50}Ni_{50}$ shape memory alloy using gold-based braze alloys. *Gold Bull.*, 39; 200-204.

Shiue, R.H., Wu, S.K. (2006b). Infrared brazing of $Ti_{50}Ni_{50}$ shape memory alloy using two Ag-Cu-Ti active braze alloys. *Intermetallics*, 14, 630-638.

Smith, N.A., Antoun, G.G., Ellis, A.B. & Crone, W.C. (2004). Improved adhesion between nickel-titanium shape memory alloy and a polymer matrix via Silane-coupling agents. *Compos. A: Appl. Sci. Manuf.*, 35, 1312-1407.

Song, G., Ma, N. & Li, H.N. (2006). Applications of shape memory alloys in civil structures. *Eng. Struct.*, 28, 1266-1274.

Song, Y.G., Li, W.S., Li, L. & Zheng, Y.F. (2008) The influence of laser welding parameters on the microstructure and mechanical property of the as-jointed NiTi alloy wires. *Mater. Lett.*, 62, 2325-2328.

Takei, F., Miura, T. & Miyazaki S. (1983). Stress-induced martensitic transformation in a Ti-Ni single crystal. *Scripta Metall. Mater.*, 17: 987-992.

Thomas, W.M.; Nicholas, E.D.; Needham, J.C.; Murch, M.G., Temple-Smith, P. & Dawes, C.J. (1991). Friction-stir butt welding, GB Patent No. 9125978.8, International patent application No. PCT/GB92/02203.

Tuissi, A., Besseghini, S., Ranucci, T., Squatrito, F. & Pozzi, M. (1999). Effect of Nd:YAG laser welding on the functional properties of Ni-49.6at% Ti. *Mater. Sci. Eng.*, A 273-275, 813-817.

Tuissi, A., Bassani, P., Gerosa, M., Mauri, D., Pini, M., Capello, E., Previtali, B. & Vedani, M. (2003). CO_2 laser welding of NiTi/Ni-based alloys. *Proc. Int. Conf. Shape Memory and Superelastic Technologies*, 2003, Pacific Grove, CA, USA, 229-238.

Villars, P., Prince, A., Okamoto, J. (1995). *Handbook of ternary alloy phase diagrams*. Metals Park, ASM International.

Wang, G. (1997). Welding of Nitinol to Stainless Steel. *Proc. 2nd Int. Conf. Shape Memory and Superelastic Technologies*, pp.131-136, Pacific Grove, CA, USA.

Wang, G.Z. (2007). A finite element analysis of evolution of stress-strain and martensite transformation in front of a notch in shape memory alloy NiTi. *Mater. Sci. Eng.*, 460-461, 383-391.

Wu, M.H. & Schetky L.McD. (2000). Industrial applications for shape memory alloys. *Proc. Int. Conf. Shape Memory and Superelastic Technologies*, pp.171-182, Pacific Grove, CA, USA, 2000.

Yan, X.J., Yang, D.Z. & Qi, M. (2006). Rotating-bending fatigue of a laser-welded superelastic NiTi alloy wire. *Mater. Charact.*, 57, 58-63.

Yan, Z., Cui, L.S. & Zheng, Y.J. (2007). Microstructure and martensitic transformation behaviours of explosively welded NiTi/NiTi laminates. *Chinese J. Aeronautics*, 27, 168-171.

Yang, T.Y., Shiue, R.K. & Wu, S.K. (2004). Infrared brazing of $Ti_{50}Ni_{50}$ shape memory alloy using pure Cu and Ti-15Cu-15Ni foils. *Intermetallics*, 12, 1285-1292.

Zhao, X.K., Wang, W., Chen, L., Liu, F., Chen, G., Huang, J. & Zhang. H. (2008). Two-stage superelasticity of a Ce-added laser-welded TiNi alloy. *Mater. Letters.*, 62, 3539-3541.

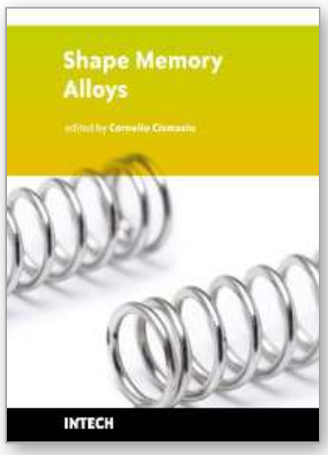
Zhao, X.K., Tang, J.W., Lan, L., Haung, J.H., Zhang, H. & Wang Y. (2009). Vacuum brazing of NiTi alloy by AgCu eutectic filler. *Mater. Sci. Technol.*, 25, 1495-1497.

Zhao, X.K., Lan, L., Sun, H., Haung, J.H., Zhang, H. & Wang, Y. (2010). Mechanical properties of additive laser welded NiTi alloy. *Mater. Letters.*, 64, 628-631.

Zhi, C.L., Xing, K.Z. & Hong, Z. (2003). Microstructure and Superelasticity of Severely Deformed TiNi Alloy. *Mater. Letters*, 57, 1086-1090.

IntechOpen

IntechOpen



Shape Memory Alloys

Edited by Corneliu Cismasiu

ISBN 978-953-307-106-0

Hard cover, 210 pages

Publisher Sciyo

Published online 18, October, 2010

Published in print edition October, 2010

In the last decades, the Shape Memory Alloys, with their peculiar thermo-mechanical properties, high corrosion and extraordinary fatigue resistance, have become more popular in research and engineering applications. This book contains a number of relevant international contributions related to their properties, constitutive models and numerical simulation, medical and civil engineering applications, as well as aspects related to their processing.

How to reference

In order to correctly reference this scholarly work, feel free to copy and paste the following:

Odd Akselsen (2010). Joining of Shape Memory Alloys, Shape Memory Alloys, Corneliu Cismasiu (Ed.), ISBN: 978-953-307-106-0, InTech, Available from: http://www.intechopen.com/books/shape-memory-alloys/joining-of-shape-memory-alloys

INTECH
open science | open minds

InTech Europe
University Campus STeP Ri
Slavka Krautzeka 83/A
51000 Rijeka, Croatia
Phone: +385 (51) 770 447
Fax: +385 (51) 686 166
www.intechopen.com

InTech China
Unit 405, Office Block, Hotel Equatorial Shanghai
No.65, Yan An Road (West), Shanghai, 200040, China
中国上海市延安西路65号上海国际贵都大饭店办公楼405单元
Phone: +86-21-62489820
Fax: +86-21-62489821

© 2010 The Author(s). Licensee IntechOpen. This chapter is distributed under the terms of the Creative Commons Attribution-NonCommercial-ShareAlike-3.0 License, which permits use, distribution and reproduction for non-commercial purposes, provided the original is properly cited and derivative works building on this content are distributed under the same license.

IntechOpen

IntechOpen